Journal of Solid State Chemistry 183 (2010) 975–983

Contents lists available at ScienceDirect

Journal of Solid State Chemistry

journal homepage: www.elsevier.com/locate/jssc

# Formation of scandium carbides and scandium oxycarbide from the elements at high-($P$, $T$) conditions

Erick A. Juarez-Arellano [a,g,*], Björn Winkler [a], Lkhamsuren Bayarjargal [a], Alexandra Friedrich [a], Victor Milman [b], Daniel R. Kammler [c], Simon M. Clark [d], Jinyuan Yan [d], Monika Koch-Müller [e], Florian Schröder [a], Miguel Avalos-Borja [f,1]

[a] Institut für Geowissenschaften, Goethe-Universität Frankfurt, Altenhöferallee 1, 60438 Frankfurt a.M., Germany
[b] Accelrys, Science Park, Cambridge, UK
[c] Sandia National Laboratories, Albuquerque, NM 87185, USA
[d] ALS, Lawrence Berkeley National Laboratory, Berkeley, CA 94720, USA
[e] GeoForschungsZentrum, Telegrafenberg Sektion 4.1, D-14473 Potsdam, Germany
[f] Centro de Nanociencias y Nanotecnologia, Universidad Nacional Autonoma de Mexico, A. Postal 2681, Ensenada, B.C., Mexico
[g] Universidad del Papaloapan, Circuito Central 200, Parque Industrial, Tuxtepec 68301, Mexico

ARTICLE INFO

*Article history:*
Received 6 November 2009
Received in revised form
19 February 2010
Accepted 27 February 2010
Available online 6 March 2010

*Keywords:*
Scandium carbides
Scandium oxycarbides
Laser-heated diamond-anvil cell
Multi-anvil press
Synchrotron
DFT calculations

ABSTRACT

Synchrotron diffraction experiments with in situ laser heated diamond anvil cells and multi-anvil press synthesis experiments have been performed in order to investigate the reaction of scandium and carbon from the elements at high-($P$,$T$) conditions. It is shown that the reaction is very sensitive to the presence of oxygen. In an oxygen-rich environment the most stable phase is $ScO_xC_y$, where for these experiments $x=0.39$ and $y=0.50$–$0.56$. If only a small oxygen contamination is present, we have observed the formation of $Sc_3C_4$, $Sc_4C_3$ and a new orthorhombic $ScC_x$ phase. All the phases formed at high pressures and temperatures are quenchable. Experimentally determined elastic properties of the scandium carbides are compared to values obtained by density functional theory based calculations.



## 1. Introduction

Transition metal carbides are an extremely interesting class of materials with very attractive properties such as high melting points, high bulk and shear moduli, and high chemical stability [1]. Due to these interesting properties a very large number of studies have appeared in the literature, with a strong emphasis on carbides formed by elements from the groups IVB, VB and VIB. In contrast, carbides of the group IIIB elements, such as scandium carbides, have received very little attention. One reason for the scarcity of studies are the experimental challenges posed by the observation that scandium is a very reactive element, which is very easily oxidised and which is difficult to refine; 99% pure scandium was not produced until 1960 [2,3].

From earlier studies it is clear that the scandium-carbon system seems to contain numerous phases, but this has not been fully explored yet. A cubic phase with composition between ScC and $ScC_2$ has a NaCl-structure type (B1) and a composition dependent lattice parameter $a=4.51$–$4.72$ Å [4–6]. Further cubic phases which have been proposed are $Sc_2C_3$ ($Pu_2C_3$-structure type with $a=7.205$ Å [6]), $Sc_4C_3$ ($Th_3P_4$-structure type, $a=7.207$ Å [7]) and $Sc_{13}C_{10}$ (unknown structure type, $a=8.53$ Å [8]). A tetragonal phase was first reported as $Sc_{15}C_{19}$ ($P\bar{4}2_1c$, $a=7.50$ Å and $c=15.00$ Å [9]) but, based on single crystal diffraction experiments, it was later concluded that the correct composition was $Sc_3C_4$, with space group $P(4/m)nc$, and lattice parameters $a=7.4873$ Å and $c=15.026$ Å [10].

It was mentioned in early reports that a stoichiometric ScC-B1 structure cannot form either due to an intrinsic non-stoichiometry or due to the possible formation of scandium oxycarbide, $Sc_2OC$ [5,11]. Nowotny and Neckel [11] supported the hypothesis of a stabilisation of the ScC-B1 structure by an oxygen incorporation based on the interpretation of band structure calculations. Conversely, it was shown experimentally [12,13] that small amounts of carbon are necessary in order to stabilise the formation of ScO-B1.

Due to the strong affinity of scandium for oxygen even nominally pure Sc metal will contain small amounts of oxygen.

* Corresponding author at: Universidad del Papaloapan, Circuito Central 200, Parque Industrial, Tuxtepec 68301, Mexico.
*E-mail address:* eajuarez@unpa.edu.mx (E.A. Juarez-Arellano).
[1] On sabbatical leave at IPICyT, San Luis Potosi, Mexico.

0022-4596/$ - see front matter © 2010 Elsevier Inc. All rights reserved.
doi:10.1016/j.jssc.2010.02.019

Karen and Hájek [14] confirmed experimentally that a stoichiometric ScC-B1 structure will not form due to the stability of mixed crystals of scandium oxycarbides $ScC_xO_y\square_{1-x-y}$ (i.e. $ScC_{0.30}O_{0.70}$ with $a=4.536(2)$ Å or $ScC_{0.56}O_{0.08}\square_{0.36}$ with $a=4.6707(4)$ Å). Karen and Hájek [14] mentioned that in an oxygen-rich environment $ScC_xO_y\square_{1-x-y}$ is in equilibrium with Sc and $Sc_2O_3$, while in a carbon-rich environment it is in equilibrium with $Sc_3C_4$.

To the best of our knowledge there has been no in situ study of the high-temperature, high-pressure behaviour of scandium carbides. Krikorian et al. [7,8] annealed arc-melted samples in a belt type press at 1.5–3 GPa and 1323–1573 K. They observed that when the starting nominal arcmelt composition was between $ScC_{0.6}$ and $ScC_{1.1}$ the stable phase after annealing was $Sc_4C_3$ while the addition of a small amount of germanium led to the formation of $Sc_{13}C_{10}$. In both cases not all reflections observed in X-ray diffraction patterns could be indexed.

The present study aims to expand our knowledge of scandium carbides by exploring their formation at high pressures and high temperatures. The reaction of the elements was investigated in situ through laser heated diamond anvil cell experiments and ex situ through multi-anvil press synthesis experiments. The recovered sample from the multi-anvil press synthesis was analysed with X-ray diffraction, electron energy loss spectroscopy (EELS), energy dispersive X-ray spectroscopy (EDS), and transmission electron microscopy EDS mapping (TEM-EDS). Further observations of the sample were made by scanning electron microscopy (SEM). The experimental studies are complemented with density functional theory (DFT) based model calculations.

## 2. Experimental details

### 2.1. Starting materials

In order to explore the scandium-carbon system at high-($P$,$T$) conditions graphite, which had previously been characterised by Winkler et al. [15], scandium foil and scandium flakes were used as starting materials. The scandium foil (Alpha Aesar, 99.9%) had a thickness of 25 μm. The flakes had previously been characterised by Kammler et al. [16] and have been obtained by cryomilling Sc metal pieces at 77 K. The presence of nitrogen in the pulverised scandium was dismissed by EELS analysis. Based on neutron diffraction experiments the oxygen content was estimated in $Sc_{0.87(6)}O_{0.13(6)}$. In all the experiments an excess of carbon was used.

### 2.2. Laser heated diamond anvil cell experiments

High pressure experiments were performed at the Advanced Light Source, ALS (Berkeley), on beam line 12.2.2 using 30 keV radiation. Double sided laser heating was performed with fibre lasers. The experimental set-up is described in detail in Caldwell et al. [17]. We employed Boehler-Almax diamond anvil cells with conical anvils and 0.35 mm culets and effective aperture of $\approx 60^\circ$. We used tungsten gaskets, preindented to 42 μm. Gasket holes with a diameter of ≈120 μm were drilled by a home-built laser lathe. We used NaCl as a pressure medium and for thermal insulation. A ruby was loaded to allow pressure determination by the ruby fluorescence method.

Due to the strong absorption of the laser radiation by the opaque samples, only moderate laser power was required to achieve bright hot spots. However, due to technical problems with the temperature determination, only approximate temperatures could be determined. Laser heating with moderate laser power (around 10–15 W per laser) leads to temperatures of about 1600–2200 K in the sample. Experience shows that the optical emission of samples which react on laser heating is very variable and a more reliable temperature determination was not possible. As the current study was aimed to observe reactions and characterise the products, this short-coming had no consequences in the present context.

Diffraction patterns were acquired with a MAR345 image plate detector. The sample-to-detector distance of 307.45 mm was determined from a $LaB_6$ reference sample. Counting times varied between 120 and 3600 s. Most data collection was done with a $10\times10\,\mu m^2$ beam spot. The laser spots had a diameter of about 30 μm. The diffraction images were processed, corrected for distortion and integrated using FIT2D [18]. Intense and well defined single-crystal diffraction spots from individual larger grains of the sample, and from the diamonds were masked manually and excluded from the integration. The background of the integrated powder diffraction patterns was extracted using the program DATLAB [19]. Le Bail fits were performed using the program FULLPROF [20] in order to obtain unit cell parameters. A linear interpolation between approximately 30 manually selected points for the background and a pseudo-Voigt profile function were used. Pressures were determined with an off-line spectrometer using the ruby fluorescence method [21] and from the known equation of state for NaCl [22] during the diffraction measurements. The two pressures determined independently from each other agreed typically within 1 GPa. Diffraction data were collected at different pressures without heating; at pressures of around 9, 14 and 18 GPa prior to heating, during heating and on temperature quenched samples. For each temperature run, a new sample position was selected.

#### 2.2.1. Multi-anvil press based synthesis

The synthesis was carried out in a multi-anvil apparatus at the GeoForschungsZentrum Potsdam using a 14/8 assembly (octahedron length/truncation length) at 10 GPa and 1673 K for 2 h. The assembly was calibrated at room temperature against the phase transitions in Bi metal [23,24]. Calibrations at higher temperature were based on the following phase transitions: $CaGeO_3$: garnet-perovskite [25]; $SiO_2$: coesite-stishovite [26]; $Mg_2SiO_4$: $\alpha-\beta$ transition [27]. A mechanical mixture of scandium (flakes) and graphite was loaded into a MgO sleeve which was enclosed in a MgO-based octahedral pressure medium within a $LaCrO_3$ heater. The temperature was controlled using a W5%Re–W26%Re thermocouple. No pressure correction was applied to the emf. The recovered sample was ground and placed in a capillary (0.3 mm inner diameter). Powder X-ray diffraction patterns were recorded at room temperature with a Panalytical XPert/MPD diffractometer. Cu$K\alpha_1$ radiation from a Cu anode operating at 45 kV and 40 mA was used.

### 2.3. Electron microscopy characterisation

SEM observations were made using a JEOL 5300 scanning electron microscope at CNyN-UNAM (Ensenda, Mexico) on the multi-anvil press recovered sample. The ground, uncoated sample was mounted on aluminium stubs with double-sided sticking carbon tape. The EDS analysis was performed with a Kevex Superdry EDS system mounted on the same JEOL 5300 microscope. Data acquisition was done through a 4PI multichannel processor interface. Great care was taken to avoid counts from the carbon sticking tape by acquiring EDS spectra at the center of large grains. Backscattered electron (BSE) images were acquired with a GW detector and an additional 4PI interface. TEM-EDS mapping was performed in a Tecnai G2 F30 operated at 300 kV, with a spherical-aberration coefficient (Cs) of 1.2 mm, at IPICyT in

San Luis Potosi (Mexico). EELS was performed with a Gatan Image Filter system mounted on the same instrument.

### 2.4. Density functional theory

Density functional theory (DFT) calculations were performed employing the CASTEP code [28]. The code is an implementation of Kohn–Sham DFT based on a plane wave basis set in conjunction with pseudopotentials. The plane-wave basis set is unbiased (as it is not atom-centered) and does not suffer from the problem of basis-set superposition error unlike atom-centered basis sets. It also makes converged results straightforward to obtain in practice, as the convergence is controlled by a single adjustable parameter, the plane wave cut-off, which we set to 330 eV. All pseudopotentials, taken from the CASTEP database, were ultrasoft and were generated using the PBE exchange-correlation functional [29] to allow for fully consistent treatment of the core and valence electrons. The Brillouin-Zone integrals were performed using Monkhorst–Pack grids [30] with spacings between grid points of less than 0.02 $Å^{-1}$. A simultaneous optimisation of the unit cell parameters and internal co-ordinates was performed so that forces were converged to 0.005 eV/Å and the stress residual to 0.005 GPa. The carbon pseudopotential has been used in several studies of transition metal carbides by us [31,15,32,33] and is known to be reliable. The Sc-pseudopotential was tested by computing the lattice parameters of scandium, and its elastic stiffness coefficients and bulk modulus by the stress–strain method. The results are given in Table 1 and the good agreement between experimental and theoretical values implies that structures and properties of scandium carbides can be reliably predicted.

**Table 1**
Comparison of experimentally determined [41] and computed structural parameters, elastic stiffness coefficients, $c_{ij}$, (from Fisher and Dever [46] as quoted by Rao and Menon [42]) and bulk modulus, $B$ of scandium. Errors given for the theoretical values are obtained from the least squares analysis of the stress–strain values.

| | Exp. | Theo. |
|---|---|---|
| $a$ (Å) | 3.309 | 3.325 |
| $c$ (Å) | 5.2733 | 5.176 |
| $c_{11}$ (GPa) | 99.3 | 106(3) |
| $c_{33}$ (GPa) | 106.9 | 106(5) |
| $c_{44}$ (GPa) | 27.7 | 30(1) |
| $c_{12}$ (GPa) | 45.7 | 40(3) |
| $c_{13}$ (GPa) | 29.4 | 31(2) |
| $B$ (GPa) | 57 | 58(1) |

## 3. Results

### 3.1. Laser heated diamond anvil cell experiments

According to McMahon et al. [34], hexagonal α-Sc transforms to an incommensurate composite structure at around 23 GPa. Therefore, in order to avoid this transition, the first DAC was loaded at around 18 GPa using scandium foil. The sample was laser heated several times trying to start the reaction without success. In rhenium carbide we have shown that pressure shifts the reaction temperature to higher values [35]. Hence, we decided to decrease the pressure in the DAC to around 9 GPa. At this pressure the reaction between α-Sc and graphite took place immediately with low laser power ( $\sim 6-8$ W per laser). Typically the low laser power we used leads to temperatures of about 1000 K. Some typical frames recorded with the MAR345 image plate detector are shown in Fig. 1. While mainly well defined rings are observed before laser heating (Fig. 1(a)), very spotty images are observed after the laser heating (Fig. 1(b)). In the recovered sample (Fig. 1(b)) several new well defined rings appeared, some of them have rather distinct high $d$-values at the center of the images. The diffraction patterns obtained before any heating could be fully indexed by an assignment of peaks to either NaCl (used for thermal insulation) or α-Sc (Fig. 2(a) and Table 2). Due to its comparatively low scattering cross section, carbon could not be detected. After the first laser heating, new reflections were observed, but it was not until the second laser heating that the intensity of the new reflections allowed us to properly index them by an assignment of peaks to the tetragonal $Sc_3C_4$ phase (Fig. 2(b)). Several non-overlapping reflections of this $Sc_3C_4$ phase can be observed in the low $2\theta$ region (Fig. 2(b)). At this stage some reflections, labeled with question marks (Fig. 2(b)), could not be indexed with any of the known scandium carbide phases reported to date.

Further laser heating at 9 GPa with higher laser power (10–12 W per laser, $\sim 1600-2000$ K) leads to the formation of several phases like the tetragonal $Sc_3C_4$, a cubic phase ($Sc_2C_3$ or $Sc_4C_3$), and several unidentified reflections (Fig. 2(c)).

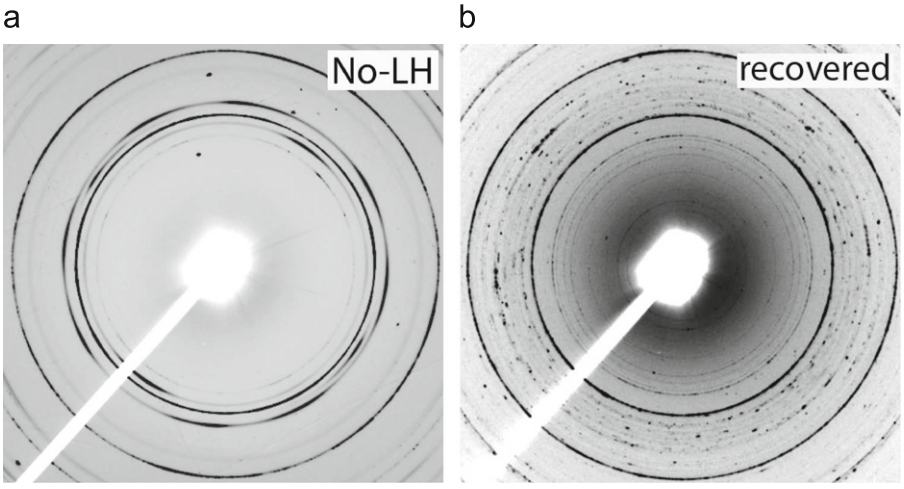


**Fig. 1.** Selected images recorded with a MAR345 image plate detector show the reaction of α-Sc (foil) and graphite. (a) Before laser heating at 9 GPa and (b) from the recovered sample.

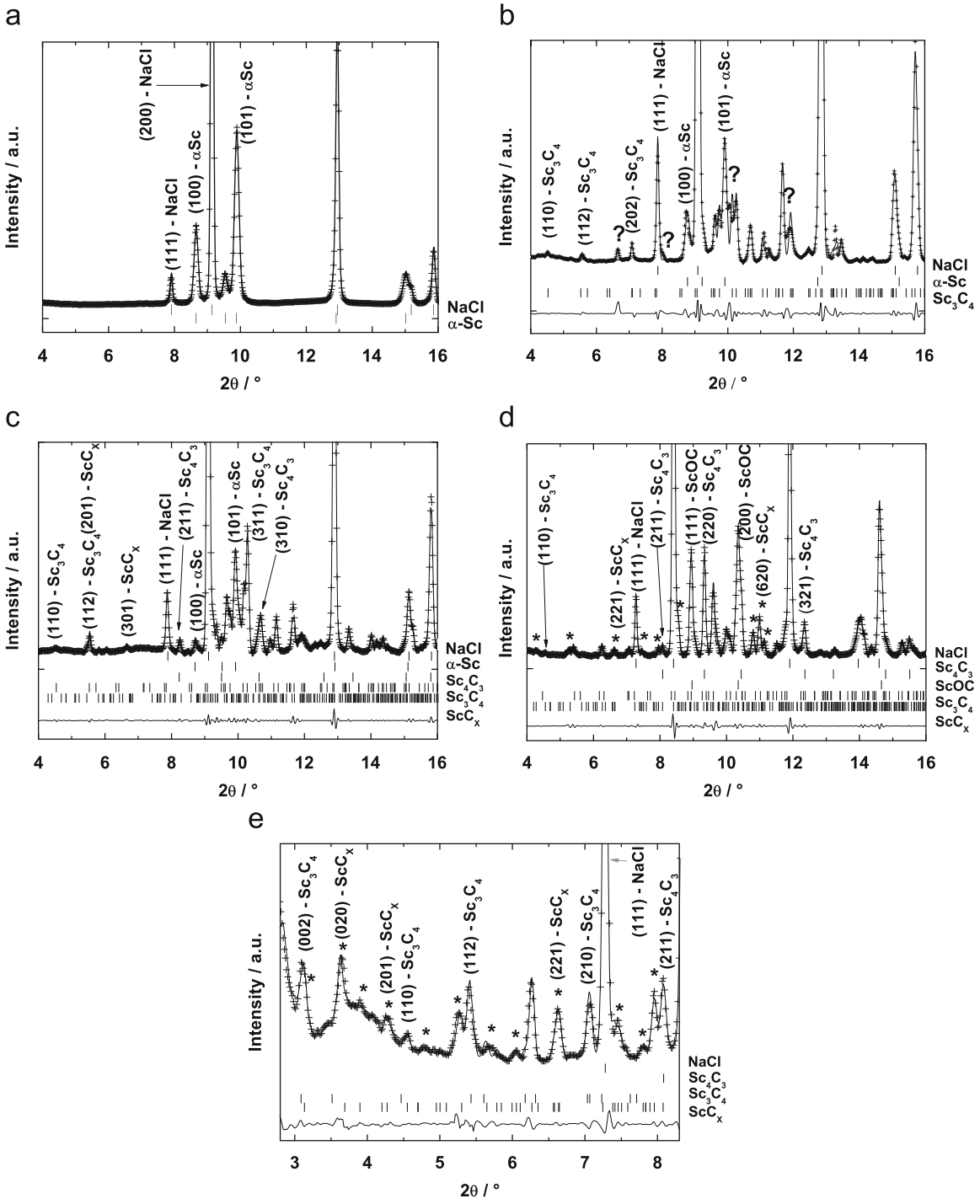


**Fig. 2.** Evolution of the reaction of α-Sc (foil) and graphite. Diffraction pattern taken at 9 GPa before laser heating (a), after the second laser heating (b), after the third laser heating (c), and from the recovered sample (d, e). The question marks and the asterisks are guides to the eyes to highlight unidentified (b) and the orthorhombic $ScC_x$ phase reflections (d, e), respectively.

The cubic phase has lattice parameters of 7.1794(4) and 7.2037(8) Å at ambient conditions, depending on the synthesis conditions (Tables 2 and 3). These values are close to the values reported for $Sc_4C_3$ ($a$=7.207 Å, Krikorian et al. [7,8]) and for $Sc_2C_3$ ($a$=7.205 Å, Rassaerts et al. [6]). In fact, both of these structures are reported to have space group symmetry $I\bar{4}3d$, and in both structures, Sc is thought to occupy Wyckoff position 16$c$ with $x \approx 0.05$. The only difference is the position of the carbon atom, which is placed on a 24$d$ position in $Sc_2C_3$ [6], and on a 12$a$ position in $Sc_4C_3$ [7,8]. In both cases, the sites are fully occupied. This raises the suspicion that in fact the same compound was studied, and that one of the structural models is incorrect. We cannot distinguish between the two structural models from our diffraction data. However, full geometry optimisations with the density functional theory based model described above, gave a lattice parameter of $a$($Sc_4C_3$, theo)=7.244 Å, in the expected agreement with the value reported in the literature, while $a$($Sc_2C_3$, theo)=7.714 Å. The often observed "underbinding" in DFT-GGA calculations such as have been performed here is expected to lead to slightly (1–3%) too large lattice parameters,

**Table 2**
Lattice parameters of the phases observed when scandium foil and graphite were laser-heated.

| $P$ (GPa) | LH | Phase | S.G. | $a$ (Å) | $b$ (Å) | $c$ (Å) | $V$ (Å$^3$) |
|---|---|---|---|---|---|---|---|
| 9 | – | NaCl | $Fm\bar{3}m$ | 5.2169(3) | – | – | 141.98(1) |
| | | α-Sc | $P\frac{6_3}{m}mc$ | 3.1802(2) | – | 4.9911(9) | 43.72(1) |
| 9 | Second | NaCl | $Fm\bar{3}m$ | 5.2124(3) | – | – | 141.70(2) |
| | | α-Sc | $P\frac{6_3}{m}mc$ | 3.1296(4) | – | 5.0132(8) | 43.32(2) |
| | | $Sc_3C_4$ | $P\frac{4}{m}nc$ | 7.3951(3) | – | 14.9640(6) | 818.34(6) |
| 9 | Third | NaCl | $Fm\bar{3}m$ | 5.2024(1) | – | – | 140.642(6) |
| | | α-Sc | $P\frac{6_3}{m}mc$ | 3.1427(2) | – | 4.9783(6) | 42.583(7) |
| | | $Sc_4C_3$ | $I\bar{4}3d$ | 7.0538(8) | – | – | 350.97(7) |
| | | $Sc_3C_4$ | $P\frac{4}{m}nc$ | 7.3845(4) | – | 14.9658(9) | 816.1(1) |
| | | $ScC_x$ | $Pmmm$ | 14.7129(9) | 11.9075(9) | 5.3798(4) | 942.5(1) |
| 14 | During | NaCl | $Fm\bar{3}m$ | 5.1425(7) | – | – | 135.99(3) |
| | | $Sc_4C_3$ | $I\bar{4}3d$ | 7.0104(9) | – | – | 344.53(8) |
| | | $Sc_3C_4$ | $P\frac{4}{m}nc$ | 7.2931(9) | – | 14.8108(9) | 787.77(9) |
| | | $ScC_x$ | $Pmmm$ | 14.4988(9) | 11.7992(9) | 5.3362(8) | 912.88(9) |
| Recovered | – | NaCl | $Fm\bar{3}m$ | 5.6364(1) | – | – | 179.065(9) |
| | | $Sc_4C_3$ | $I\bar{4}3d$ | 7.1794(4) | – | – | 370.05(3) |
| | | $ScO_xC_y$ | $Fm\bar{3}m$ | 4.5804(2) | – | – | 96.072(6) |
| | | $Sc_3C_4$ | $P\frac{4}{m}nc$ | 7.4990(6) | – | 15.0260(9) | 844.98(9) |
| | | $ScC_x$ | $Pmmm$ | 15.1169(9) | 12.1528(7) | 5.5386(3) | 1017.58(7) |

**Table 3**
Lattice parameters of the phases observed when scandium flakes and graphite were laser-heated.

| $P$ (GPa) | LH | Phase | S.G. | $a$ (Å) | $c$ (Å) | $V$ (Å$^3$) |
|---|---|---|---|---|---|---|
| 13 | Before | NaCl | $Fm\bar{3}m$ | 5.1254(2) | – | 134.65(1) |
| | | α-Sc | $P\frac{6_3}{m}mc$ | 3.1527(8) | 4.880(3) | 42.01(3) |
| | | W | $Im\bar{3}m$ | 3.1364(5) | – | 30.853(9) |
| 13 | During | NaCl | $Fm\bar{3}m$ | 5.1521(4) | – | 137.03(2) |
| | | α-Sc | $P\frac{6_3}{m}mc$ | 3.1344(3) | 4.983(1) | 42.40(1) |
| | | W | $Im\bar{3}m$ | 3.141(3) | – | 30.98(3) |
| | | $Sc_4C_3$ | $I\bar{4}3d$ | 7.015(2) | – | 345.3(1) |
| | | $ScO_xC_y$ | $Fm\bar{3}m$ | 4.5101(7) | – | 91.74(3) |
| 13 | After | NaCl | $Fm\bar{3}m$ | 5.1521(7) | – | 136.76(1) |
| | | α-Sc | $P\frac{6_3}{m}mc$ | 3.1358(7) | 4.9828(9) | 41.97(1) |
| | | W | $Im\bar{3}m$ | 3.1276(4) | – | 30.59(4) |
| | | $Sc_4C_3$ | $I\bar{4}3d$ | 7.0124(4) | – | 344.8(4) |
| | | $ScO_xC_y$ | $Fm\bar{3}m$ | 4.4889(9) | – | 90.45(7) |
| | | $Sc_3C_4$ | $P\frac{4}{m}nc$ | 7.3356(2) | 14.8487(9) | 799.0(6) |
| Recovered | – | NaCl | $Fm\bar{3}m$ | 5.6349(1) | – | 178.831(6) |
| | | W | $Im\bar{3}m$ | 3.1602(2) | – | 31.563(4) |
| | | $Sc_4C_3$ | $I\bar{4}3d$ | 7.2037(8) | – | 373.83(4) |
| | | $ScO_xC_y$ | $Fm\bar{3}m$ | 4.5980(3) | – | 97.27(1) |
| | | $Sc_3C_4$ | $P\frac{4}{m}nc$ | 7.5085(5) | 14.9845(9) | 844.78(2) |

but an overestimation by more than 7% is a very strong indication that the underlying structural model is problematic.

DFT model calculations show that in a carbon saturated environment the left-hand side of the reaction

$$Sc_4C_3 + 3C \leftrightarrows 2Sc_2C_3 \quad (1)$$

is more stable by 0.13 eV. In a scandium saturated environment, the reaction energy for the reaction

$$Sc_4C_3 \leftrightarrows Sc_2C_3 + 2Sc \quad (2)$$

shows $Sc_4C_3$ to be much more stable by 1.88 eV. Hence, we conclude that a cubic compound with $a \approx 7.2$ Å is very probably $Sc_4C_3$ (Fig. 2(c)).

The unidentified reflections were labeled as an unknown $ScC_x$ phase and indexed with an orthorhombic unit cell with cell parameters $a=14.7194(7)$ Å, $b=11.9111(7)$ Å, and $c=5.3862(4)$ Å (Table 2) using the Dicvol program [36] (Fig. 2(c)). Due to the absence of systematic extinctions, the space group *Pmmm* (IT 47) was chosen. An enlargement of the low $2\theta$ region of the diffraction pattern from the recovered sample shows several distinct and non-overlapping reflections which we assigned to this new orthorhombic $ScC_x$ phase (Fig. 2(e)). These reflections can also be observed in the two-dimensional detector image shown in Fig. 1(b). Hence we believe that the lattice parameters we obtained are reliable (Table 2).

Further laser heating at 9 GPa or at 14 GPa with different laser power neither caused a decomposition of the already formed phases, nor promotes the formation of any other phase, independent whether we studied regions of the sample which had been reacted before at lower pressures, or regions in which there was still α-Sc present.

Once the laser heating was completed, the pressure was released and the gasket was taken out of the DAC before collecting data of the recovered sample (Figs. 2(d) and (e)). All the phases observed at high-($P$,$T$) conditions were quenchable. In addition, in the recovered sample we detected small amounts of an extra phase which could be indexed by assigning them to $ScO_xC_y$. The lattice parameter and its significance for the oxygen contamination is discussed below.

A second DAC was loaded using scandium flakes and pressurised to 13 GPa. The diffraction patterns obtained before any heating could be fully indexed by an assignment of peaks to

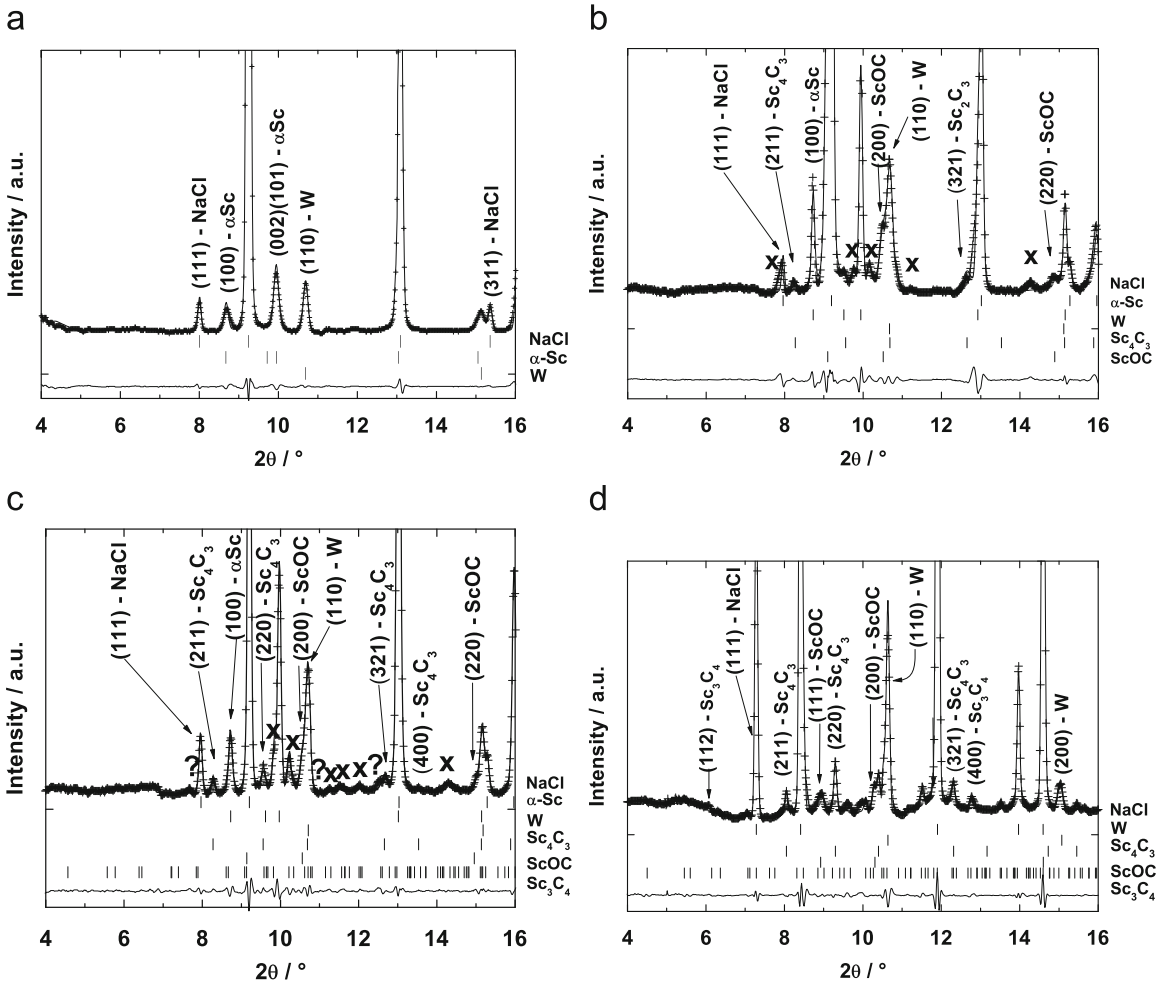


**Fig. 3.** Evolution of the reaction of α-Sc (flakes) and graphite. Diffraction patterns taken at 13 GPa before laser heating (a), during laser heating (b) and after laser heating (c), and from the recovered sample (d). The X markers (b, c) and question marks (c) are guides to the eyes to highlight $Sc_3C_4$ and unidentified reflections, respectively.

either NaCl (used in the thermal insulation), W (gasket material) or α-Sc (Fig. 3(a) and Table 3). The reaction of α-Sc and carbon was detected during laser heating (laser power of $\sim 7-12$ W per laser) by the formation of the cubic phases $ScO_xC_y$ and $Sc_4C_3$, and the appearance of unidentified reflections (Fig. 3(b)). After laser heating, the diffraction pattern could be almost completely indexed by an assignment of reflections to $ScO_xC_y$, $Sc_4C_3$ and $Sc_3C_4$. Only very few reflections remained unindexed (Fig. 3(c)). Within our detection limits, we did not observe any trace of the orthorhombic $ScC_x$ phase we found in the first experiment. Further laser heating with different laser power did not decompose the already formed phases, or promote the formation of any other phase. All the phases observed at high-($P$,$T$) conditions were quenchable (Fig. 3(d)).

### 3.2. Multi-anvil press synthesis

Four phases were identified in the recovered multi-anvil press sample: MgO (impurity from the surrounding capsule material), graphite, diamond and $ScO_xC_y$ (Fig. 4 and Table 4). The observed transformation from graphite to diamond agrees with the pressure–temperature carbon phase diagram [37]. Within our detection limits neither α-Sc nor any of the other carbide phases observed in the DAC experiments ($Sc_4C_3$, $Sc_3C_4$ or the orthorhombic $ScC_x$) were observed in the X-ray diffraction pattern (Fig. 4).

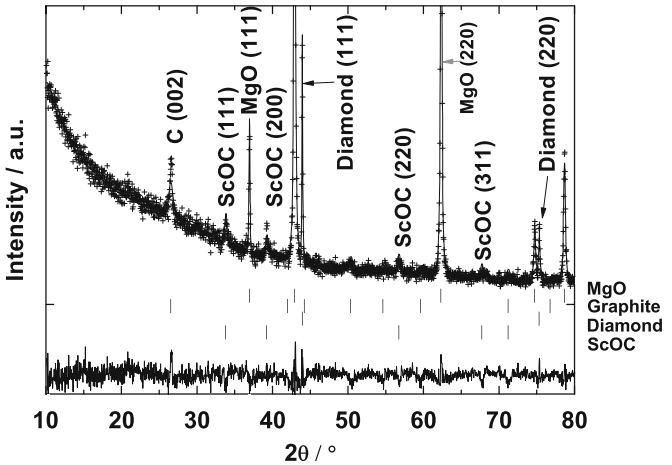


**Fig. 4.** X-ray powder diffraction pattern from the recovered sample synthesised in a multi-anvil press at 10 GPa and 1673 K.

The formation of the $ScO_xC_y$ phase can be explained by the oxygen present in the scandium flakes and the oxygen-rich environment provided by the surrounding capsule material (MgO).

To further characterise the recovered sample from the multi-anvil press synthesis, the sample was studied by SEM and TEM.

*3.2.1. SEM and TEM characterisation of the sample recovered from the multi-anvil press synthesis*

A typical SEM image representative of the sample is shown in Fig. 5(a). The sample consists of an agglomeration of two kinds of homogeneous particles with diameters between 3 and 10 μm. An image of the same area using backscattered electrons in compositional mode shows that the sample is made up of two compounds (Fig. 5(b)). In this mode, bright areas correspond to regions enriched with elements with higher atomic number. An EDS analysis of the bright area indicates a scandium rich compound (Fig. 5(c)) while the dark regions are pure carbon. TEM-EDS mapping over a small particle of the bright areas shows that the distribution of scandium, carbon and oxygen is homogeneous (Fig. 5(d)). The oxygen content in small particles of $SiO_2$ (mill mortar residues) observed in the TEM-EDS mapping can be used as a reference for the distribution of oxygen in the recovered sample. EELS spectra in the low energy window (Fig. 6(a)), also from the bright area and with no support interference, shows the zero-loss peak and the bulk plasmon peak (~14 eV). The scandium high order $M_{2,3}$ core-loss edge onset was located at ~39 eV. This spectrum is different from that of the pure scandium spectrum reported by Cukier et al. [38]. Our spectra are similar to the scandium oxide EELS spectra reported by Cukier et al. [38], but the shapes and relative intensities are different, as could be expected, as our sample is an oxycarbide, instead of a pure oxide. In a high energy window, besides the carbon K and the scandium $L_2L_3$ peaks, the oxygen K-peaks can be observed (Fig. 6(b)). Several EELS spectra were taken on different particles and the peaks associated with oxygen were present in all of them. Therefore, these results confirm the presence of oxygen in the sample and thus the formation of scandium oxycarbide in the multi-anvil press synthesis. A quantitative interpretation of the EELS spectra was, however, beyond the scope of the present study.

**Table 4**
Lattice parameters of the structures observed in the recovered sample from the multi-anvil press experiment at 10 GPa and 1673 K using scandium flakes.

| Phase | S.G. | $a$ (Å) | $c$ (Å) | $V$ (Å$^3$) | |
|---|---|---|---|---|---|
| MgO | $Fm\bar{3}m$ | 4.2096(1) | – | 74.596(4) | This study |
| MgO | $Fm\bar{3}m$ | 4.2114 | – | 74.69 | [43] |
| Graphite | $P\frac{6_3}{m}mc$ | 2.4805(7) | 6.7124(9) | 35.77(2) | This study |
| Graphite | $P\frac{6_3}{m}mc$ | 2.464 | 6.711 | 35.29 | [44] |
| Diamond | $Fd\bar{3}m$ | 3.5651(2) | – | 45.313(4) | This study |
| Diamond | $Fd\bar{3}m$ | 3.5669 | – | 45.38(4) | [45] |
| $ScO_xC_y$ | $Fm\bar{3}m$ | 4.5833(7) | – | 96.28(3) | This study |
| $ScO_xC_y$ | $Fm\bar{3}m$ | 4.51–4.72 | – | 92–105 | [4–6] |

## 4. Discussion and conclusions

Irrespective of the starting material used and the experiment performed, the lattice parameters obtained from all the recovered phases are very similar to the values reported in the literature. Some of these values can therefore be used as an internal standard and allow an estimate of the accuracy of our results (Tables 2–4). Specifically, our values for the lattice parameters of NaCl, W, MgO and diamond agree to within 0.1% with literature values (i.e. NaCl: 5.6401 Å [39] and W: 3.1648 Å [40]).

The unit cell parameters of $Sc_4C_3$ and $Sc_3C_4$ (Tables 2 and 3) determined by us agree to within 0.4% with literature values ($a$=7.207 Å [7]; $a$=7.4873 Å and $c$= 15.026 Å [10], respectively). This small variation in the lattice parameters may be due to small differences in the carbon contents of the samples, which, however, we cannot quantify.

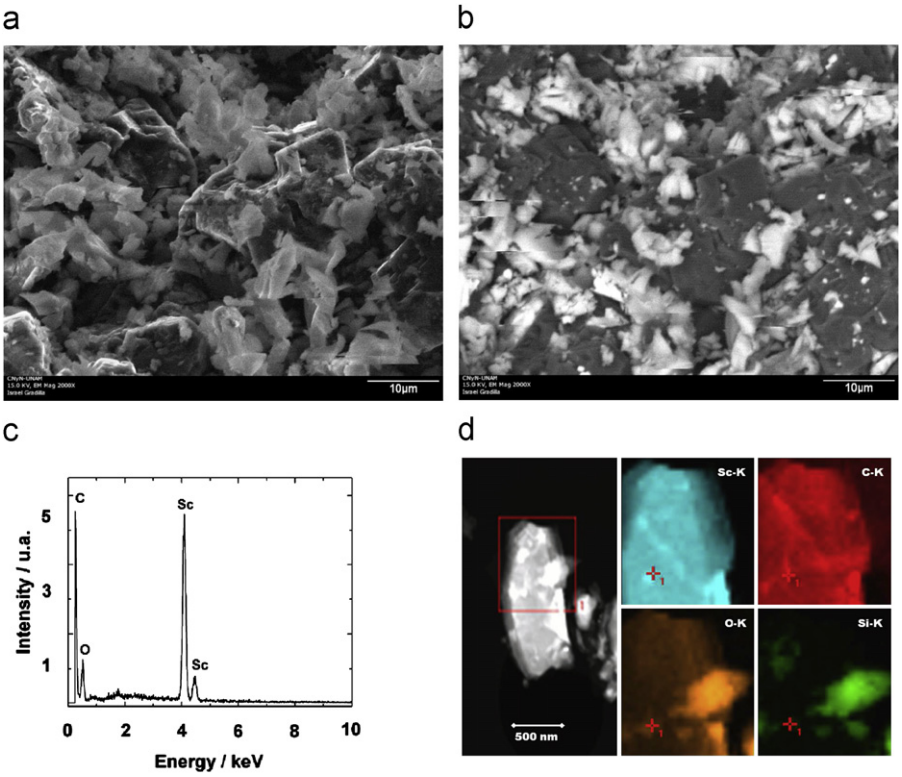


**Fig. 5.** Recovered sample from the multi-anvil press synthesis. (a) SEM image (secondary electrons) shows that the sample is formed of particles with diameters between 3 and 10 μm. (b) BSE image (compositional mode) shows the co-existence of two phases. (c) EDS from the bright area shows a scandium rich compound. (d) TEM-EDS mapping over the bright areas shows the distribution of scandium, carbon and oxygen.

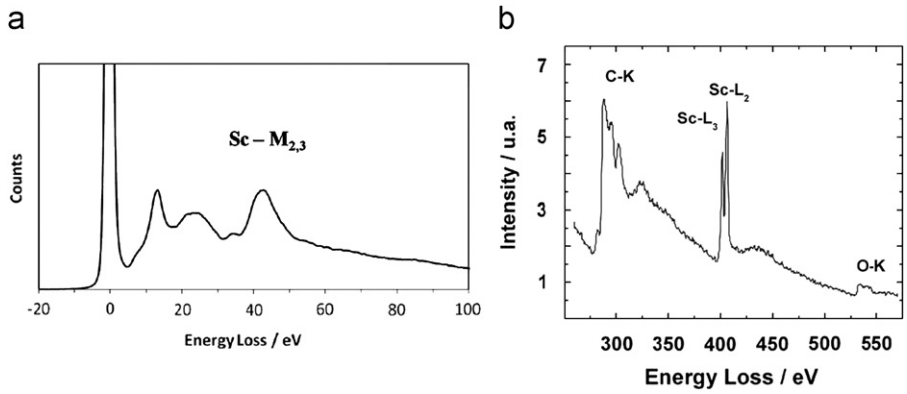


**Fig. 6.** Recovered sample from the multi-anvil press synthesis. (a) EELS spectra in the low energy window show the zero-loss peak, the bulk plasmon peak ($\sim$14 eV) and the scandium high order $M_{2,3}$ core-loss edge onset ($\sim$39 eV). (b) EELS from a high energy window shows peaks associated with carbon, scandium and oxygen. An $SiO_2$-contamination (from the mortar) can be identified and is the origin of the bright part in the image showing the oxygen distribution.

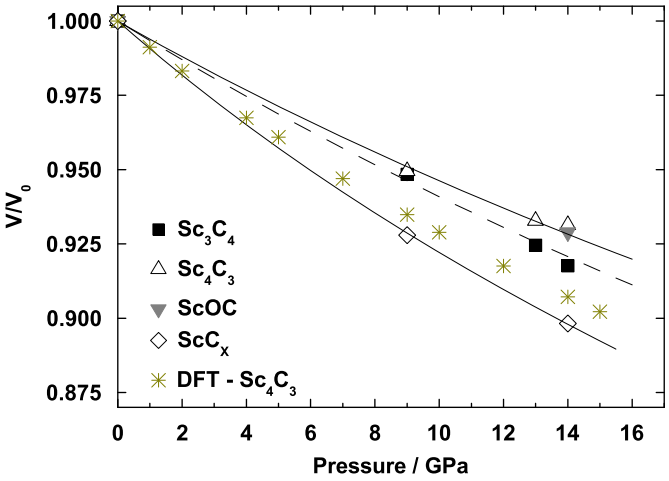


**Fig. 7.** Variation of the normalised unit cell volumes as a function of pressure of scandium carbides obtained during the LH-DAC experiments. Lines represent BM-EOS fits to the experimental results.

**Table 5**
Bulk moduli from fits of 2nd-order Birch–Murnaghan equations of state to the LH-DAC experimental data, and theoretical elastic properties obtained by DFT calculations.

| | $V_0$ (Å$^3$) | $B_0$ (GPa) |
|---|---|---|
| $Sc_4C_3$, exp | 370.2(3) | 157(2) |
| $Sc_4C_3$, DFT | 380.2 | 105(3) |
| $Sc_3C_4$, exp | 863.5(5) | 144(3) |
| $Sc_3C_4$, DFT | 837.6 | 140(1) |
| $ScO_xC_y$, exp | 97.46(1) | 190(90) |
| ScC-B1, DFT | 103.4 | 160(3) |
| ScO-B1, DFT | 91.1 | 183(1) |
| $ScC_x$, exp | 1017.7(1) | 105(1) |

**Table 6**
Elastic stiffness coefficients, $c_{ij}$ (GPa) from DFT calculations.

| | $c_{11}$ | $c_{33}$ | $c_{44}$ | $c_{66}$ | $c_{12}$ | $c_{13}$ |
|---|---|---|---|---|---|---|
| $Sc_3C_4$ | 280(1) | 274(1) | 76.3(5) | 103.4(1) | 65.1(3) | 74(2) |
| $Sc_4C_3$ | 218(6) | – | 65(3) | – | 49(1) | – |
| ScC (B1) | 330(5) | – | 63.4(3) | – | 75(3) | – |
| ScO (B1) | 390(2) | – | 58.6(3) | – | 79(1) | – |

In the present study we have shown that scandium oxycarbide is readily formed at high pressures. Specifically, the observation that in a high pressure experiment in an oxygen rich environment (our multi-anvil synthesis) only scandium oxycarbide was formed, with no presence of a scandium carbide, indicates the high relative stability of the scandium oxycarbide with respect to a carbide in the presence of oxygen. In the DAC experiments, the available amount of oxygen is much more limited than in the multi-anvil cell experiments, and only then a multi-phase assemblage is observed. It is interesting to note that the unit cell parameters of the $ScO_xC_y$ phases observed in the recovered samples is similar irrespective of the starting material used and the experiment performed (Tables 2–4). A comparison of the unit cell parameters of the $ScO_xC_y$ phases we have synthesised with those published by Karen and Hájek [14] imply that our samples have compositions between $ScO_{0.39}C_{0.50}$ and $ScO_{0.39}C_{0.56}$.

To the best of our knowledge, we have determined the pressure dependence of any of the scandium carbides for the first time. As the focus of the present study was on sample synthesis, we only could obtain data at a few pressures and hence the analysis was limited to a fit with a 2nd-order Birch–Murnaghan equation of state. The pressure dependencies of the normalised unit cell volumes of $Sc_3C_4$, $Sc_4C_3$, $ScO_xC_y$ and the new orthorhombic $ScC_x$ are shown in Fig. 7, the corresponding bulk modulus values are listed in Table 5. Theoretical values based on the DFT model calculations are also given in Table 5. These values have been derived from calculated values of the elastic stiffness coefficients, reported in Table 6.

Due to the scarcity of data, the experimental value for the bulk modulus of the scandium oxycarbide has a very large error bar. In those cases we can compare DFT results with experimental data, the bulk moduli obtained from the DFT models are always lower. This is due to the well known "underbinding" generally observed in DFT-GGA calculations, which have been mentioned above. Despite these differences, all data taken together allow to conclude that the carbides are of intermediate compressibility, similar to e.g. silicate garnets. The oxides are always less compressible, e.g. $B(ScO) > B(ScC)$.

We conclude that the knowledge of the Sc–C–O system as a function of pressure and temperature is still incomplete, an indication for this is that we have observed a previously unknown orthorhombic phase. Further, our DFT results convincingly show that $Sc_2C_3$ probably does not exist and that the correct composition is $Sc_4C_3$.

In summary, the current study has shown that scandium carbides and scandium oxycarbide offer a rich field for future investigations and that these compounds are as interesting as the intensively studied group IVB and group VB carbides.

## Acknowledgments

This research was supported by Deutsche Forschungsgemeinschaft (Project Wi-1232), in the framework of the DFG-SPP 1236. E.A.JA thanks the CONACyT and A.F. thanks the CNV-Foundation for financial support. The Advanced Light Source is supported by the Director, Office of Science, Office of Basic Energy Science, of the U.S. Department of Energy under contract DE-AC02-05CH11231. This research was partially supported by COMPRES, the Consortium for Materials Properties Research in Earth Science under NSF Cooperative Agreement EAR 06-49658, by DGAPA-UNAM grant IN-108908 and by CONACyT-DAAD PROALMEX grant. Sandia is a multiprogram laboratory operated by Sandia Corporation, a Lockheed Martin Company, for the United States Department of Energy (DoE) under Contract no. DE-AC04-94AL85000.

## References

[1] H.O. Pierson, Handbook of Refractory Carbides, Noyes Publication, 1996.
[2] R.C. Weast, S.M. Selby, C.D. Hodgman (Eds.), Handbook of Chemistry and Physics, 46th ed., The Chemical Rubber Co., 1965.
[3] E.V. Galoshina, V.P. Dyakina, V.E. Startsev, The Physics and Metals and Metallography 83 (1996) 248–263.
[4] H. Nowotny, H. Auer-Welsbach, Monatshefte für Chemie 92 (1961) 789–793.
[5] H. Auer-Welsbach, H. Nowotny, Monatshefte für Chemie 92 (1961) 198–201.
[6] H. Rassaerts, H. Nowotny, G. Vinek, F. Benesovsky, Monatshefte für Chemie 98 (1967) 460–468.
[7] N.H. Krikorian, A.L. Bowman, M.C. Krupka, G.P. Arnold, High Temperature Science 1 (1969) 360–366.
[8] N.H. Krikorian, A.L. Giorgi, E.G. Szklarz, M.C. Krupka, Journal of the Less-Common Metals 19 (1969) 253–257.
[9] H. Jedlicka, H. Nowotny, F. Benesovsky, Monatshefte für Chemie 102 (1971) 389–403.
[10] R. Pöttgen, W. Jeitschko, Inorganic Chemistry 30 (1991) 427–431.
[11] H. Nowotny, A. Neckel, Journal of the Institute of Metals 97 (1969) 161.
[12] V. Dufek, F. Petrù, V. Brožek, Monatshefte für Chemie 98 (1967) 2424–2430.
[13] V. Dufek, V. Brožek, F. Petrù, Monatshefte für Chemie 100 (1969) 1628–1630.
[14] P. Karen, B. Hájek, Journal of the Less-Common Metals 120 (1986) 337–344.
[15] B. Winkler, D.J. Wilson, S.C. Vogel, D.W. Brown, T.A. Sisneros, V. Milman, Journal of Alloys and Compounds 441 (2007) 374–380.
[16] D.R. Kammler, M.A. Rodriguez, R.G. Tissot, D.W. Brown, B. Clausen, T.A. Sisneros, Metallurgical and Material Transactions A 39A (2008) 2815–2819.
[17] W. Caldwell, M. Kunz, R. Celestre, E.E. Domning, M.J. Walter, D. Walker, J. Glossinger, A.A. MacDowell, H.A. Padmore, R. Jeanloz, S.M. Clark, Nuclear Instruments and Methods in Physics Research A 582 (2007) 221–225.
[18] A.P. Hammersley, S.O. Svensson, M. Hanfland, A.N. Fitch, D. Hauserman, High Pressure Research 14 (1996) 235–248.
[19] K. Syassen, Datlab. version 1.37d, MPI/FKF Stuttgart, Germany, 2005.
[20] J. Rodriguez-Carvajal, Physica B 192 (1993) 55–69.
[21] H. Mao, P. Bell, J. Shaner, D. Steinberg, Journal of Applied Physics 49 (1978) 3276–3283.
[22] M. Chall, B. Winkler, P. Blaha, K. Schwarz, Journal of Physical Chemistry B 104 (2000) 1191–1197.
[23] E.C. Lloyd, U.S. National Bureau Standards Special Publication 326 (1971) 1–3.
[24] G.J. Piermarini, S. Block, Reviews of Scientific Instruments 46 (1975) 973–980.
[25] J.I. Susaki, M. Akaogi, S. Akimoto, O. Shimoura, Geophysical Research Letters 12 (1985) 729–732.
[26] M. Akaogi, H. Yusa, K. Shiraishi, T. Suzuki, Journal of Geophysical Research 100 (1995) 337–347.
[27] H. Morishima, T. Kato, M. Suto, E. Ohtani, S. Urakawa, W. Utsumi, O. Shimomura, T. Kikegawa, Science 265 (1994) 1202–1203.
[28] S.J. Clark, M.D. Segall, C.J. Pickard, P.J. Hasnip, M.I.J. Probert, K. Refson, M.C. Payne, Zeitschrift für Kristallographie 220 (2005) 567–570.
[29] J.P. Perdew, K. Burke, M. Ernzerhof, Physical Review Letters 77 (1996) 3865–3868.
[30] H. Monkhorst, J.D. Pack, Physical Review B 13 (1976) 5188–5192.
[31] L. Lopez-de-la Torre, B. Winkler, J. Schreuer, K. Knorr, M. Avalos-Borja, Solid State Communications 134 (2005) 245–250.
[32] B. Winkler, E.A. Juarez-Arellano, A. Friedrich, L. Bayarjargal, J. Yan, S.M. Clark, Journal of Alloys and Compounds 478 (2009) 392–397.
[33] E.A. Juarez-Arellano, B. Winkler, A. Friedrich, L. Bayarjargal, V. Milman, J. Yan, S.M. Clark, Journal of Alloys and Compounds 481 (2009) 577–581.
[34] M.I. McMahon, L.F. Lundegaard, C. Hejny, S. Falconi, R.J. Nelmes, Physical Review B 73 (2006) 134102.
[35] E.A. Juarez-Arellano, B. Winkler, A. Friedrich, D.J. Wilson, M. Koch-Müller, K. Knorr, S.C. Vogel, J.J. Wall, H. Reiche, W. Crichton, M. Ortega-Aviles, M. Avalos-Borja, Zeitschrift für Kristallographie 223 (2008) 492–501.
[36] A. Boultif, D. Louer, Journal of Applied Crystallography 37 (2004) 724–731.
[37] F.P. Bundy, Physica A 156 (1989) 169–178.
[38] M. Cukier, B. Gauthe, C. Wehenkel, Journal de Physique 41 (1980) 603–613.
[39] D. Walker, P. Verma, L. Cranswick, R. Jones, S.M. Clark, S. Buhre, American Minerologist 89 (2004) 204–210.
[40] M. Straumanis, Journal of Applied Physics 30 (1959) 1965–1969.
[41] F.H. Spedding, A.H. Daane, K.W. Herrmann, Acta Crystallographica 9 (1956) 559–563.
[42] R.R. Rao, C.S. Menon, Solid State Communications 12 (1973) 527–528.
[43] N.G. Schmahl, J. Barthel, G.F. Eikerling, Zeitschrift für Anorganische und Allgemeine Chemie 332 (1964) 230–237.
[44] P. Trucano, R. Chen, Nature 258 (1975) 136–137.
[45] T. Hom, W. Kiszenik, B. Post, Journal of Apply Crystallography 8 (1975) 457–458.
[46] E.S. Fisher, D. Dever, Proceedings 7th Rare Earth Research Conference 1 (1968) 237.